ACS MEASUREMENT SCIENCE Au
AN OPEN ACCESS JOURNAL OF THE AMERICAN CHEMICAL SOCIETY

pubs.acs.org/measureau
Perspective

Plasmon Enhanced IR Spectroelectrochemistry

Published as part of ACS Measurement Science Au special issue "2024 Rising Stars".

Jian Li,*[,§] Jin Li,[§] and Xing-Hua Xia*

Cite This: *ACS Meas. Sci. Au* 2024, 4, 606−614
Read Online
ACCESS | Metrics & More | Article Recommendations

ABSTRACT: Plasmon-enhanced infrared (IR) techniques have garnered significant interest for their ability to achieve greatly more sensitive IR detection than conventional surface enhanced IR techniques. However, the difficulty in electrically connecting antennas has limited their application in IR spectroelectrochemistry, a crucial field for catalysis, analysis, and energy storage. Recent technical advancements have enabled the successful application of electrochemical potentials to antennas, making plasmon-enhanced IR spectroelectrochemistry feasible. This perspective aims to summarize the latest strategies and offer insights into future improvements for better design of plasmon enhanced IR spectroelectrochemistry platforms and understanding of IR spectroelectrochemistry.

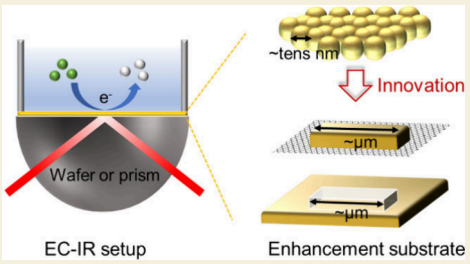

KEYWORDS: *Surface enhanced IR spectroscopy, IR spectroelectrochemistry, Plasmon, Antenna, Sensitivity*

INTRODUCTION

Infrared (IR) energy corresponds to the vibrations and rotations of chemical bonds, providing detailed molecular information. IR spectroelectrochemistry (EC-IR, schematically illustrated in Figure 1) allows in situ IR analysis of electrochemical reactions, offering unique molecular insights into reaction processes and mechanisms.[1−8] To enhance IR sensitivity at electrochemical interfaces, surface-enhanced IR spectroscopy (SEIRAS) has been developed, demonstrating signal enhancement factors (EFs) of 10−100. This has enabled the elucidation of mechanisms for electrocatalytic processes such as CO_2 reduction reactions (CO_2RRs),[8−10] nitrogen reduction reactions (NRRs),[4,11] and bioelectrochemical processes like protonation/deprotonation.[12] However, conventional EC-SEIRAS uses metallic nanofilms (shown in Figure 1) composed of nanoparticles as enhancement substrates, which exhibit weak light−matter interactions due to the mismatch between the nanoparticle size and the IR wavelength. This results in poor confinement of IR light and moderate IR enhancement, making it difficult to monitor short-lived intermediates and trace-level analytes with small cross sections.

Recently, plasmon-enhanced IR spectroscopy (PEIRS) techniques have been developed to address the sensitivity issue in SEIRAS.[13−15] These techniques use mid-IR localized surface plasmon resonance (LSPR) to significantly improve light−matter interactions and enhance the electromagnetic near field, resulting in higher IR signal enhancement. Compared to attenuated total reflectance (ATR)-SEIRAS, well-defined plasmonic structures of specific shapes and sizes (Figure 1c,d) are applied in PEIRS, efficiently concentrating the incident IR light into intense "hot spots", significantly amplifying the IR signal of target molecules with an EF of up to 10^6.[6,16,17] PEIRS techniques have shown remarkable sensitivity and have been successfully used for in situ detection of lipids, proteins, DNA, and small molecules in bioanalysis.[14,15,18−23] They can also be designed to couple with other external methods, such as fluid control and pump−probe measurement, providing unprecedented molecular insights with improved sensitivity.[24,25] Integrating plasmon-enhanced IR techniques into IR spectroelectrochemistry would greatly improve the sensitivity. As EC-IR is performed in a liquid environment with strong IR absorption, IR light should impinge from the substrate side that supports the electrode rather than propagate inside the electrolyte (Figure 1). Meanwhile, although plasmonic materials, such as metals and graphene, are generally conductive, the plasmonic structures are typically discrete on the substrate. Connecting these plasmonic structures with conductive elements such as continuous metallic films may strongly inhibit IR light penetration from the substrate side. Achieving electrical conductivity between plasmonic structures poses a core challenge for designing effective plasmon-enhanced IR spectroelectrochemistry platforms.

Since last year, two types of plasmon-enhanced IR spectroelectrochemistry (EC-PEIRS) platforms (shown in Figure 1c,d) have been proposed to address the conductivity

Received: July 25, 2024
Revised: October 8, 2024
Accepted: October 9, 2024
Published: October 21, 2024

https://doi.org/10.1021/acsmeasuresciau.4c00048
ACS Meas. Sci. Au 2024, 4, 606−614

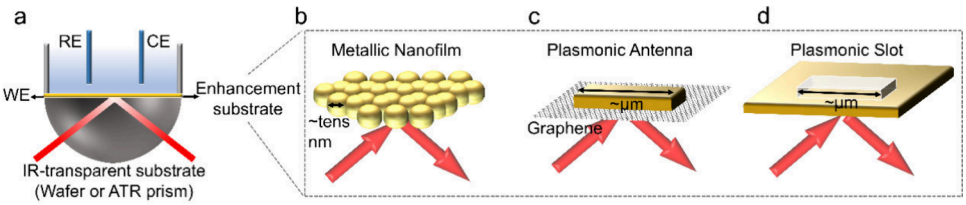

Figure 1. Schematic illustration of (a) reflectance mode EC-IR setup and (b–d) different kinds of enhancement substrates.

issue, enabling simultaneous recording of electrochemical and plasmon-enhanced EC-IR signals. One configuration uses an IR-transparent and conductive substrate to connect the antennas without significantly affecting their resonance. This allows plasmon resonance excitation from the substrate side without attenuating the incident light. Li et al.[26] employed nanosphere lithography to fabricate wafer-scale metallic triangle antennas on monolayer graphene supported by a SiO_2/Si wafer, which supports the collection of IR spectroelectrochemistry signal by applying an electrochemical potential on graphene (Figure 2). The effect of graphene on the antenna resonance was minimized using defect-free single-layer graphene. And graphene thinner than two monolayers has been proven to have no obvious IR spectral features and insignificant influence on the resonance spectra of the antenna array in electrochemical analysis.[26,27] A real IR signal enhancement factor over 1900 was attained, allowing reconstruction of electrochemical curves using IR signals (Figure 2e,f). This reconstruction, based on real-time IR absorbance directly related to current density, bypasses the limitation of detecting small currents in traditional electrochemical methods and shows potential for analyzing electrochemical processes that occur within small areas.

Using this configuration, the electrochemical CO_2 reduction reaction on the Au antenna surface was investigated. Benefitting from the high enhancement, the intermediate CO was detected at extremely low reduction current density. Two IR features were observed, which were attributed to CO adsorbed on 2-fold (CO_B) and multifold (CO_M) bridge Au sites. The variation trend of CO_B and CO_M signals implies an evolution of the active sites with applied potentials and thus provides an important supplement to the prevalent understanding of CO_2RR.

The second configuration involves using mesh-like structures. The metallic mesh itself provides electrical connectivity, and its IR enhancement can be optimized according to Babinet's principle. This principle states that if a structure has a resonance in transmission (or reflection) under a certain polarization of incident light, its inverse structure with the same geometrical parameters will have a similar resonance in reflection (or transmission) under a 90° change in polarization.[28,29] Utilizing this principle, the Krischer group[30,31] have fabricated nanoslots as the inverse structure of nanorods as plasmonic structures (Figure 3). The nanoslots are fabricated on a CaF_2 ATR prism to further increase light utilization, are tuned to enhance electromagnetic near-fields due to the excitation of a magnetic dipole aligned parallel to the slot's long axis, and create a strong, extended hotspot of the electric field within the slot. Consequently, compared to rod-type antennas, these inverse structures provide superior sensitive detection of molecular signals due to their more extended hotspots and linearly decaying electromagnetic near-fields.

Using this configuration, they studied CO adsorption and oxidation on Pt.[30] Two peaks were resolved for CO_{linear} which could be attributed to the adsorption of CO on Pt(111) and Pt(100). During the electrochemical oxidation of CO, a classic Stark effect was observed. Then, they developed a multiband nanophotonic–electrochemical platform that simultaneously monitors in situ multiple adsorbed species and studied the electrochemical reduction of CO_2 on a Pt surface, achieving an EF of ∼40 compared to results on an unstructured Pt film (Figure 2e–j).[31] Two vibrational bands of CO were observed at ∼2030 and ∼1840 cm^{-1} in a CO-saturated environment. However, during the CO_2RR in K_2CO_3, CO adsorbed in a bridged configuration could not be detected.

FEATURES OF PLASMON-ENHANCED IR SPECTROELECTROCHEMISTRY

Although still in its early stages, EC-PEIRS has demonstrated specific advantages over conventional EC-SEIRAS methods:

High Enhancement

Electrochemical interfaces often involve short-lived intermediates with low concentrations. High enhancement improves the ability to observe these intermediates, leading to a better understanding of the interfacial reaction mechanisms. Unlike rough metallic nanofilms, plasmonic structures exhibit extreme electric field confinement at specific wavelengths, significantly enhancing the signal and enabling the detection of trace-level analytes.

The signal enhancement depends on the electromagnetic near-field enhancement and the coupling between the molecular vibration and the plasmon resonance of the antennas. Efforts to enhance near-field intensity are often directed toward adjusting the structure of plasmonic antennas.[32−34] However, antenna design in IR spectroelectrochemistry is limited by macroscale fabrication methods and the need to maintain a conductive substrate. For EC-PEIRS platforms, photoetching and electron-beam lithography methods used for inverse antennas provide accurate and controllable structures, resulting in better sensitivity, but these methods are relatively expensive and complex.[30,31] Nanosphere lithography offers a convenient and relatively cheap method for fabricating well-ordered antenna arrays, yet the shape and the accuracy of the antenna structure are limited.[26]

In addition, it is crucial to match the plasmon resonance with the molecular vibration mode of interest.[35,36] Mismatched resonances will not enhance the signal, so predesigning the system resonance to align with target molecular vibrations is necessary.

High Stability

Stability ensures consistent measurement conditions and supports long-term analysis. In conventional EC-SEIRAS, metallic nanofilms are fabricated on Si or ZnSe prisms by sputtering or electroless deposition. Although films deposited

https://doi.org/10.1021/acsmeasuresciau.4c00048
ACS Meas. Sci. Au 2024, 4, 606−614

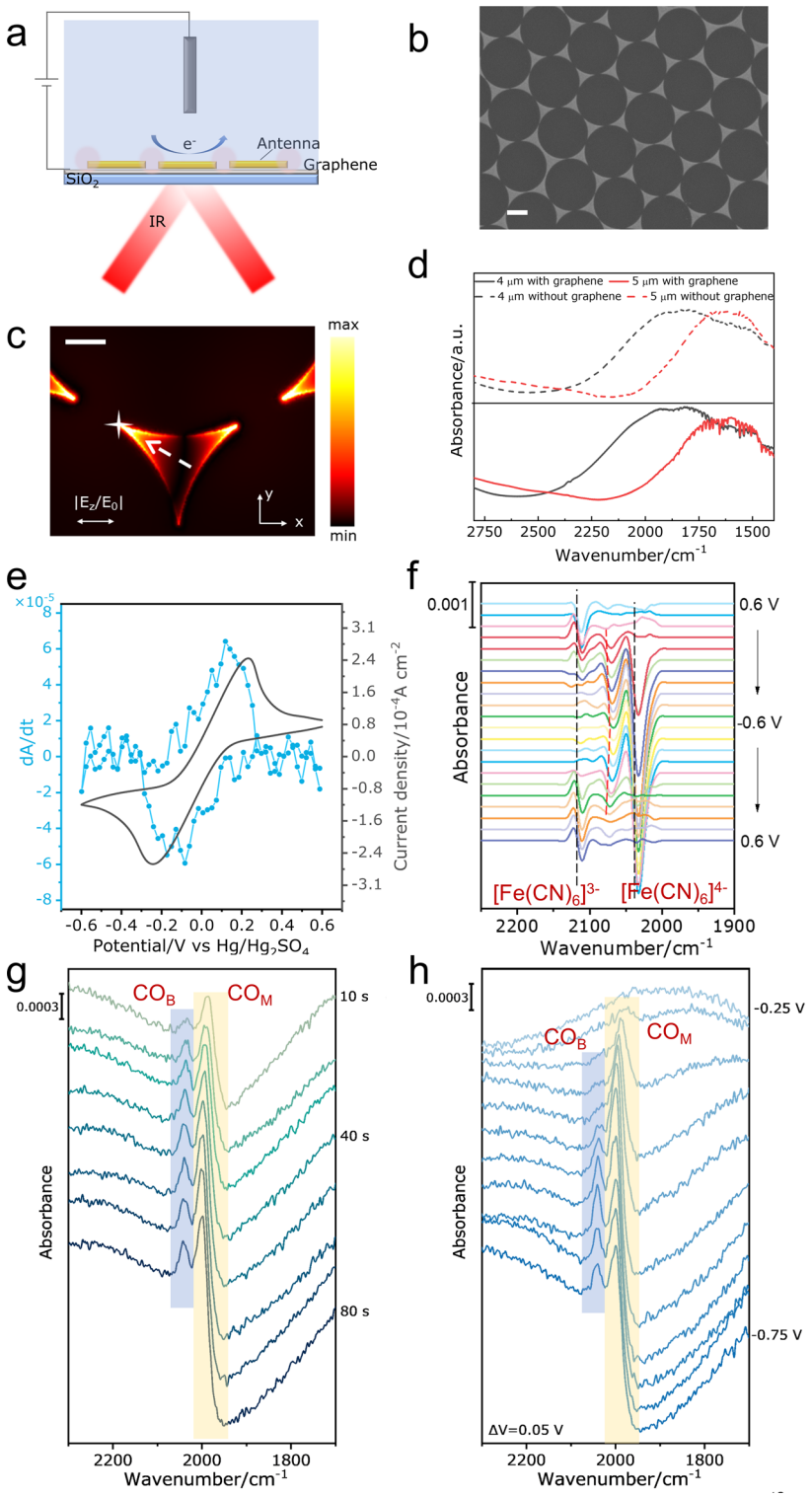

Figure 2. Plasmon enhanced IR spectroelectrochemistry on plasmonic antenna platform. (a) Schematic illustrations of the EC-PEIRS platform. (b) SEM image of a Au triangle antenna array fabricated with a 5.0 μm polystyrene (PS) sphere mask. Scale bar: 2 μm. (c) Simulation of $|E_z/E_0|$ distribution at 2000 cm^{-1} on the antenna array fabricated with a 4.0 μm PS sphere mask. (d) Measured plasmon resonance spectra of the Au antenna arrays fabricated with 4.0 and 5.0 μm PS sphere masks on graphene/SiO_2/Si and SiO_2/Si substrates. Incident angle: 8.4°. (e) Cyclic voltammogram of 5 mM $K_3Fe(CN)_6$ + 0.5 M KNO_3 solution on the EC-PEIRS platform (black curve) and the reconstructed optical signal derived curve (blue curves). (f) Real-time potential-dependent PEIRS spectra of 5 mM $K_3Fe(CN)_6$ + 0.5 M KNO_3 solution on the Au antenna array during potential cycling from 0.6 V to −0.6 V (vs Hg/Hg_2SO_4). The peaks of $[Fe(CN)_6]^{3-}$ and $[Fe(CN)_6]^{4-}$ are indicated by the dashed lines. (g) PEIRS spectra of CO produced on Au antennas at −0.65 V_{RHE} for different reduction time and captured at 0.4 V_{RHE} for 30 s in a CO_2-saturated solution of 0.5 M $NaHCO_3$. (h) PEIRS spectra of CO produced on Au antennas at different reduction potentials for 80 s and captured at an observation potential of 0.4 V_{RHE} for 30 s in a CO_2-saturated solution of 0.5 M $NaHCO_3$. Reprinted with permission from ref 26. Copyright 2024 Wiley-VCH GmbH.

https://doi.org/10.1021/acsmeasuresciau.4c00048
ACS Meas. Sci. Au 2024, 4, 606−614

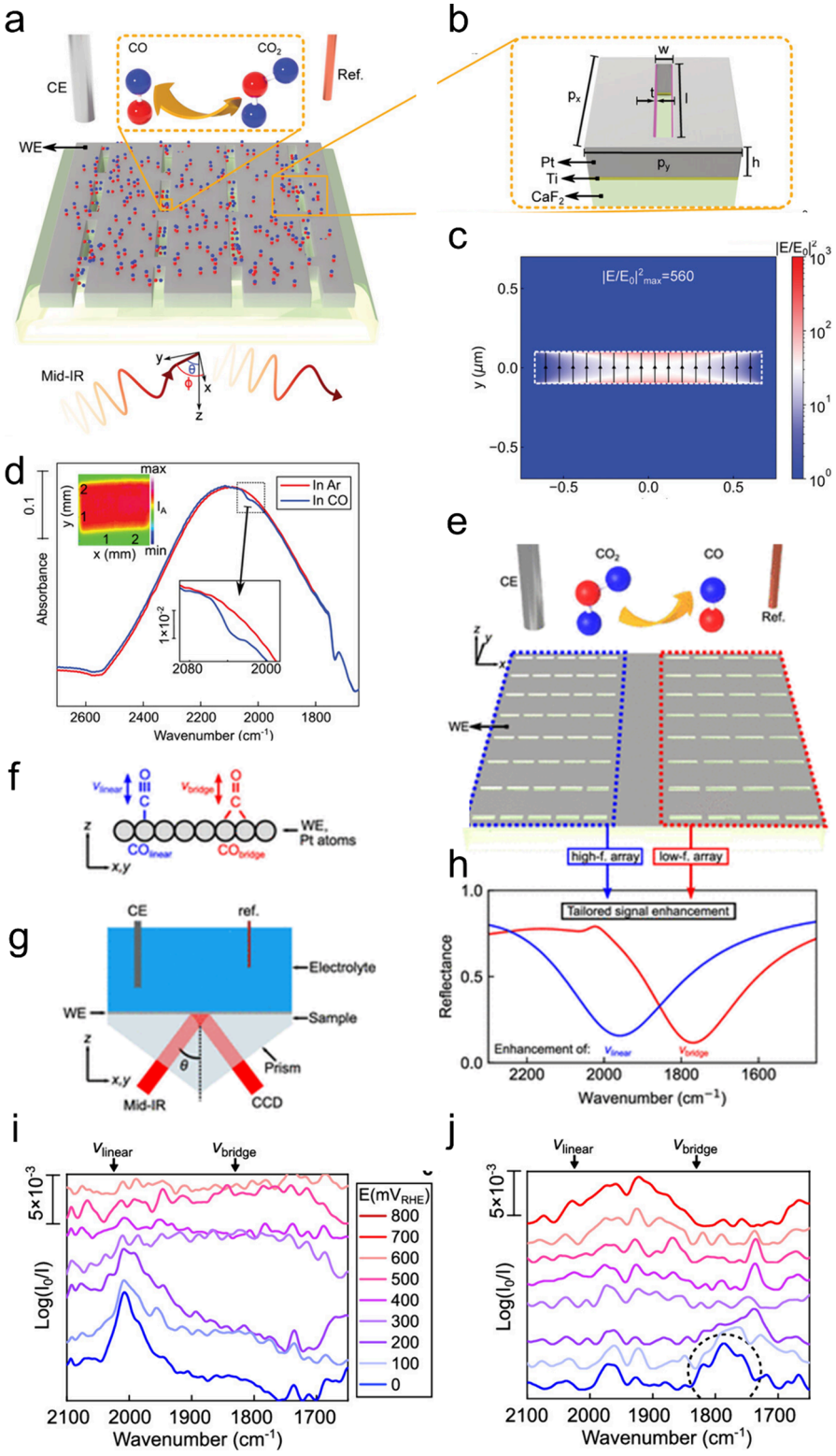

Figure 3. Plasmon enhanced IR spectroelectrochemistry on plasmonic slot platform. (a) Schematic for the Pt-based nanoslot for IR electrochemistry. (b) Sketch of the Pt on CaF_2 nanoslot unit cell. (c) Simulated electric near field intensity across the nanoslot. (d) FTIR spectra taken with s-polarized light of the Pt nanoslot/electrolyte interface in Ar and CO saturated electrolytes, respectively. Reprinted with permission under a Creative Commons CC-BY 4.0 from ref 30. Copyright 2023 Wiley-VCH GmbH. (e) Schematic of the multiband platinum-based nanoslot metasurface. The metasurface contained a high-frequency (high-*f*) and low-frequency (low-*f*) array. (f) Schematic showing the chemical structure of the two adsorption configurations of CO on platinum. (g) Schematic illustrating the metasurface in an electrochemical chamber filled with electrolyte that was illuminated from below in an ATR geometry. (h) Resonances stemming from two metasurface arrays on Pt. (i, j) Evolution of IR spectra with the potential acquired on the (i) high-frequency array optimized for CO_{linear} and (j) low-frequency array optimized for CO_{bridge} detection during the cathodic scan. Reprinted with permission under a Creative Commons CC-BY 4.0 from ref 31. Copyright 2024 American Chemical Society.

https://doi.org/10.1021/acsmeasuresciau.4c00048
ACS Meas. Sci. Au 2024, 4, 606−614

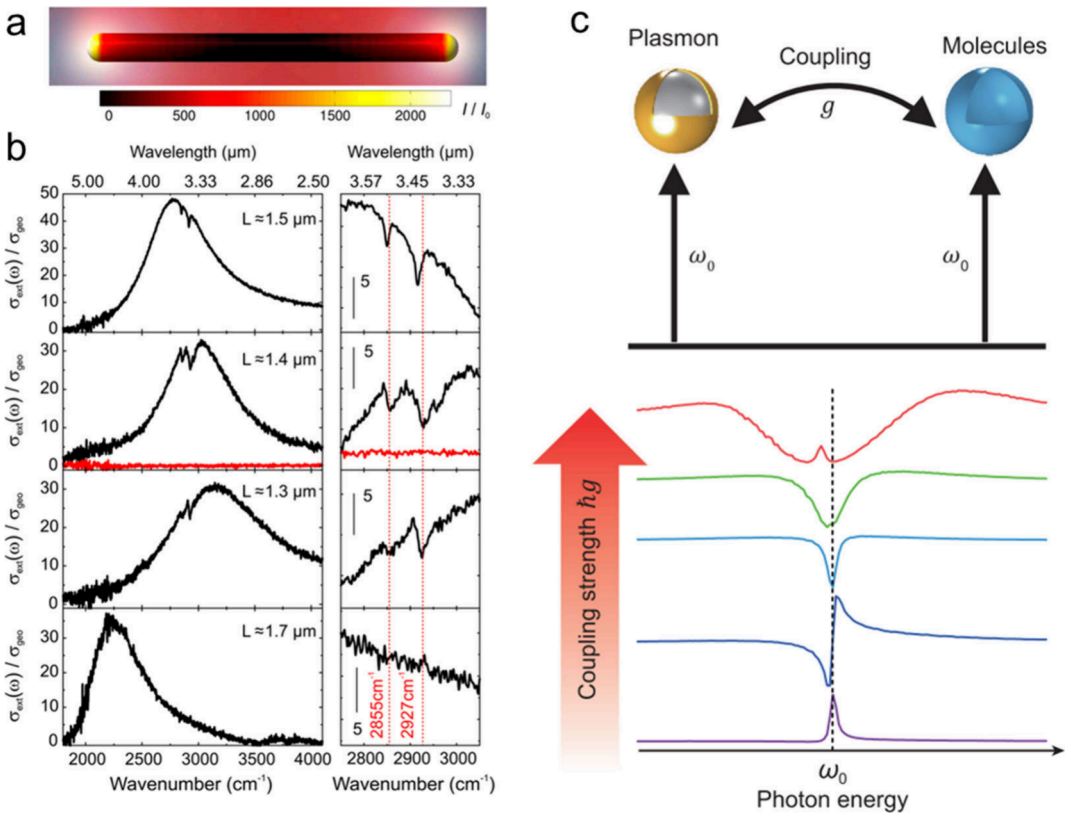

Figure 4. (a) Simulated near-field intensity on a resonant gold nanowire. (b) Experimental extinction cross sections σ_{ext} for four octadecanethiol-coated wires with different plasmon resonances. Right panels: magnifications of the vibrational signals. Reprinted with permission from ref 35. Copyright 2008 the American Physical Society. (c) Energy diagram of a resonant molecule−plasmon coupling system. The molecular vibration and plasmonic modes are both resonant with a frequency of ω_0. The bottom panel shows the typical absorption spectra of vibrational modes under various coupling strengths. Reprinted with permission under a Creative Commons CC-BY 4.0 from ref 36. Copyright 2020 Oxford University Press on behalf of China Science Publishing & Media Ltd.

by electroless deposition have stronger adhesion than sputtered films, their stability still cannot be maintained in long-term analysis, especially in electrochemical reactions with gas bubbles. As for EC-PEIRS, antennas are usually fabricated on a substrate coated with an adhesion layer, significantly improving stability.[30,31] However, the properties of this adhesion layer may affect electrochemical reactions when exposed to the electrolyte. One strategy to avoid this influence is to fabricate antennas on chemically inert graphene using electron beam evaporation. The antennas on graphene have been demonstrated to be stable during long-term electrochemical treatments.[26] Moreover, even though the metallic structure will not fall off of the substrate, it is important that the IR enhancement can remain constant despite tiny geometric changes during long-term electrochemical reactions. The size of the antenna is in the micrometer range to match IR light, making EC-PEIRS less susceptible to effects of nanoscale metal reconstruction caused by oxidation and reduction, gas bubbles, and other factors during electrochemical processes. In contrast, EC-ATR-SEIRAS enhancement relies on the morphology of closely packed particles at nanoscale size, making it more vulnerable to subtle geometric changes.

High Repeatability

Repeatability is crucial for reliable data, especially for quantitative analysis of parallel experiments. Antennas fabricated using templates and physical methods provide higher repeatability compared to rough nanofilms fabricated with chemical methods. Physically deposited antennas can be precisely controlled by varying the deposition rates and times. In contrast, metal growth in the chemical deposition process is stochastic, leading to poor repeatability. Moreover, since metallic electrodes usually need electrochemical cleaning before detection, the change of the antenna structure and enhancement resulting from this process may further lower their repeatability. This nanoscale structural evolution has less effect on antennas with microscale geometries supporting that enhancement primarily occurs at hotspots.

Broad Materials Choices for Application

The metallic structures in EC-SEIRAS usually need to function as both the electrode and catalyst, requiring a diverse range of materials for the broad investigation of electrochemical reactions. In the mid-IR region, most metals have similar optical properties due to negative real parts of their dielectric functions[37,38] and thus are potential candidates for the fabrication of enhancement substrates, showing broad materials choice. However, in EC-ATR-SEIRAS, the chemical reduction processes of electroless deposition limit material choices and complicate electrochemical maintenance, sometimes necessitating secondary deposition. In contrast, antenna fabrication does not face these limitations, with physical methods allowing a broader range of materials in EC-PEIRS and opening rich electrode materials for analysis. Additionally, EC-PEIRS can support and detect thicker samples as the enhanced field at hotspots extends beyond the near-surface

https://doi.org/10.1021/acsmeasuresciau.4c00048
ACS Meas. Sci. Au 2024, 4, 606−614

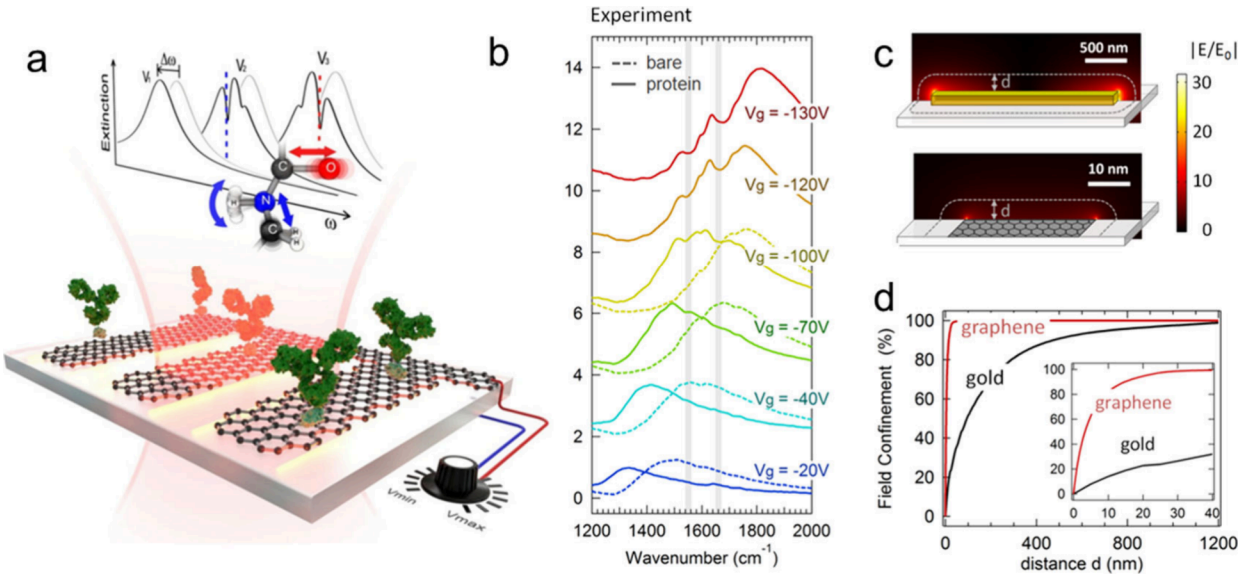

Figure 5. Graphene plasmon enhanced IR spectroscopy. (a) Graphene−plasmon-based biosensor. The presence of proteins induces a plasmon resonance spectral shift ($\Delta\omega$), accompanied by narrow dips corresponding to the molecular vibration bands of the protein, which are used for sensing. (b) Extinction spectra of a graphene nanoribbon array before (dashed curves) and after (solid curves) protein bilayer formation with different gate voltages (V_g). (c) Near-field enhancement distribution $|E/E_0|$ in the gold antenna and graphene nanoribbon operating at a resonance frequency of 1600 cm^{-1}. (d) Percentage of space-integrated near-field intensity confined within a volume extending a distance d outside the different antennas. The inset shows a zoom-in for distance between 0 and 40 nm. Reprinted with permission from ref 41. Copyright 2015 The American Association for the Advancement of Science.

electric field typical of nanofilms, which is also promising to investigate electrochemically active materials loaded on the antennas.

FUTURE IMPROVEMENT AND PERSPECTIVES

Economic Fabrication

Electroless deposition of nanofilms is cheap and fast and is applied in ambient air on the substrate scale. In contrast, antenna fabrication is more expensive and time-consuming, involving resource-intensive processes such as predesign (resonance simulation), mask fabrication, graphene deposition and transfer, metal structure fabrication, and mask removal, especially for large-area fabrication. Cost-effective and efficient fabrication methods are essential to improving the economic feasibility of these systems.

A potential cost-saving approach is to utilize chip substrates in the plasmon internal reflectance mode[18,22,24,26] rather than the ATR prism used in EC-ATR-SEIRAS. To guarantee a well-ordered antenna array geometry, the substrate surface is required to be extremely flat. Thus, although ATR mode can be more efficient with low optical loss, the high cost and the need for frequent surface repolishing of ATR prisms are not suitable for large-scale production. By focusing on the plasmon internal reflectance mode, we can reduce costs while maintaining effective performance.

Matching of Plasmon Resonance with Molecular Vibrations

Unlike nanofilms, plasmonic antennas exhibit wavelength-dependent resonance, leading to nonhomogeneous enhancement across the entire IR spectral range (Figure 4a,b). This wavelength dependence complicates the broadband spectral collection. To address this issue, it is crucial to integrate multiband/broadband resonances in one single chip. One approach is to adjust the structures of the antenna arrays. For example, a resonance multiplexing approach using a self-similar design with plasmonic rod antennas of different lengths can achieve plasmon resonances throughout the mid-IR, while placing a resonance in the near-IR for refractometric detection.[39,40] Duportal et al. applied this method to inverse antennas and established a multiband nanophotonic−electrochemical platform.[31] Alternatively, tunable materials such as graphene, phase-change materials, or conductive polymers controlled by external fields can help tune the plasmon resonance to cover a wider spectral range and extend spectral collection.[41−43] However, the intrinsic tuning effects of electrochemical potentials applied to these materials need careful evaluation to avoid interference.

The strong dipole of the plasmon resonance can have different coupling efficiencies with the molecular vibrational dipole, complicating accurate interpretation of acquired IR signals (Figure 4c). For example, in EC-ATR-SEIRAS, the weak coupling of nanofilms enhances IR absorption across the entire IR spectral range with a positive peak in absorbance, sometimes resulting in a bipolar peak when nanoparticles become larger with stronger confinement.[44,45] This Fano-shaped peak is more prominent in PEIRS, which can also show a negative peak due to the more effective coupling between antenna resonance and molecular vibration. Generally, the signal strength is quantified as the difference between the minimum and maximum of the Fano peak.[20,46] For quantitative analysis, an adaptation of the asymmetric least-squares smoothing method proposed by Eilers[47] can be applied for baseline correction to remove plasmon resonance from the measured spectra.[20,26,46,48] However, once coupling reaches the strong coupling regime, Rabi splitting makes interpreting signals challenging, as slight shifts in molecular vibration can produce significantly different results.[49] While physical models and numerical analysis can theoretically analyze plasmon resonance and coupling phenomena with known molecular

https://doi.org/10.1021/acsmeasuresciau.4c00048
ACS Meas. Sci. Au 2024, 4, 606−614

properties and amounts, it is often difficult to preidentify intermediates and their optical properties and amounts. Applying these models to real conditions requires careful consideration. Experienced modeling techniques combined with AI-assisted methods could greatly aid in achieving accurate understanding and application.[50]

Improved Sensitivity

Achieving better signal enhancement is crucial for capturing and understanding key intermediates and expanding the range of materials and applications. Plasmonic antennas offer superior signal enhancement potential due to their more effective ability to confine electromagnetic fields compared to traditional nanofilms. Precise design of antenna shape, size, and periodicity can achieve high performance. For instance, Dong et al.[17] employed bow tie shaped junction nanoantennas with gaps smaller than 3 nm, demonstrating the highest theoretical SEIRA enhancement to date with an EF of 10^7. However, the average EF is significantly reduced when the material is arranged in an antenna array. A high density of hot spots in the detection area is essential for practical application.

Another promising alternative is using plasmons on graphene for EC-PEIRS, which confines fields near the antenna surface, providing high enhancement sensitive to the electric double layer very close to the electrode (Figure 5).[41,43,51] However, the effect of electrochemical potential on graphene's resonance, which changes the Fermi level, should be considered.

A significant challenge arises from the mismatch between the effective IR active spot and the electrochemical active spot. In microelectrodes, the electrochemical reaction can occur across the entire antenna or even the entire metallic surface of the nanoslot. However, the IR detection region of EC-PEIRS is mainly in the hotspots. This mismatch complicates the precise interpretation of EC-PEIRS results and should be addressed in future works.

CONCLUSIONS

In conclusion, EC-PEIRS holds great promise for investigating electrochemical processes with enhanced sensitivity, potentially uncovering mechanisms beyond the scope of conventional EC-ATR-SEIRAS. This early perspective offers a comprehensive overview of the current and ongoing developments in EC-PEIRS techniques for EC-IR investigation. Designing and applying new EC-PEIRS platforms for specific systems could provide deeper insights into electrochemical mechanisms and guide the design of improved properties.

AUTHOR INFORMATION

Corresponding Authors

Jian Li − *State Key Lab of Analytical Chemistry for Life Science, School of Chemistry and Chemical Engineering, Nanjing University, Nanjing 210023, China;* orcid.org/0000-0002-1682-1685; Email: jianli@nju.edu.cn

Xing-Hua Xia − *State Key Lab of Analytical Chemistry for Life Science, School of Chemistry and Chemical Engineering, Nanjing University, Nanjing 210023, China;* orcid.org/0000-0001-9831-4048; Email: xhxia@nju.edu.cn

Author

Jin Li − *State Key Lab of Analytical Chemistry for Life Science, School of Chemistry and Chemical Engineering, Nanjing University, Nanjing 210023, China*

Complete contact information is available at: https://pubs.acs.org/10.1021/acsmeasuresciau.4c00048

Author Contributions

[§]Jian Li and Jin Li contributed equally to this work. CRediT: **Jian Li** conceptualization, funding acquisition, project administration, writing - original draft, writing - review & editing; **Jin Li** conceptualization, funding acquisition, writing - original draft, writing - review & editing; **Xing-Hua Xia** conceptualization, funding acquisition, project administration, writing - original draft, writing - review & editing.

Notes

The authors declare no competing financial interest.

ACKNOWLEDGMENTS

This work was supported by grants from the National Natural Science Foundation of China (22227806, 22374074, 22004069), the Natural Science Foundation of Jiangsu Province, China (BK20241232), the Fundamental Research Funds for the Central Universities (2024300444), and the Excellent Research Program of Nanjing University (ZYJH004).

REFERENCES

(1) Nishikawa, Y.; Fujiwara, K.; Ataka, K.; Osawa, M. Surface-Enhanced Infrared External Reflection Spectroscopy at Low Reflective Surfaces and its Application to Surface-Analysis of Semiconductors, Glasses, and Polymers. *Anal. Chem.* **1993**, *65* (5), 556−562.

(2) Ataka, K.; Giess, F.; Knoll, W.; Naumann, R.; Haber-Pohlmeier, S.; Richter, B.; Heberle, J. Oriented Attachment and Membrane Reconstitution of His-Tagged Cytochrome C Oxidase to a Gold Electrode: in situ Monitoring by Surface-Enhanced Infrared Absorption Spectroscopy. *J. Am. Chem. Soc.* **2004**, *126* (49), 16199−16206.

(3) Li, J.; Zheng, B.; Zhang, Q.-W.; Liu, Y.; Shi, C.-F.; Wang, F.-B.; Wang, K.; Xia, X.-H. Attenuated Total Reflection Surface-Enhanced Infrared Absorption Spectroscopy: A Powerful Technique for Bioanalysis. *J. Anal. Test.* **2017**, *1*, 8.

(4) Yao, Y.; Zhu, S.; Wang, H.; Li, H.; Shao, M. A Spectroscopic Study on the Nitrogen Electrochemical Reduction Reaction on Gold and Platinum Surfaces. *J. Am. Chem. Soc.* **2018**, *140* (4), 1496−1501.

(5) Li, S.; Wu, L.; Liu, Q.; Zhu, M.; Li, Z.; Wang, C.; Jiang, X.; Li, J. Uncovering the Dominant Role of an Extended Asymmetric Four-Coordinated Water Network in the Hydrogen Evolution Reaction. *J. Am. Chem. Soc.* **2023**, *145* (49), 26711−26719.

(6) Hou, J.; Xu, B.; Lu, Q. Influence of Electric Double Layer Rigidity on CO Adsorption and Electroreduction Rate. *Nat. Commun.* **2024**, *15* (1), 1926.

(7) Chao, Y.; Li, H.; Jiang, T.-W.; Huang, J.-A.; Ma, X.-Y.; Jiang, K.; Cai, W.-B. Recent Advancements of Electrochemical Attenuated Total Reflection Surface-Enhanced Infrared Absorption Spectroscopy. *Curr. Opin. Electrochem.* **2024**, *46*, No. 101509.

(8) Wei, Y.; Mao, Z.; Jiang, T. W.; Li, H.; Ma, X. Y.; Zhan, C.; Cai, W. B. Uncovering Photoelectronic and Photothermal Effects in Plasmon-Mediated Electrocatalytic CO_2 Reduction. *Angew. Chem., Int. Ed.* **2024**, *63* (13), No. e202317740.

(9) Yang, K.; Kas, R.; Smith, W. A. In situ Infrared Spectroscopy Reveals Persistent Alkalinity near Electrode Surfaces during CO_2 Electroreduction. *J. Am. Chem. Soc.* **2019**, *141* (40), 15891−15900.

(10) Malkani, A. S.; Anibal, J.; Xu, B. Cation Effect on Interfacial CO_2 Concentration in the Electrochemical CO_2 Reduction Reaction. *ACS Catal.* **2020**, *10* (24), 14871−14876.

(11) Yao, Y.; Zhu, S. Q.; Wang, H. J.; Li, H.; Shao, M. H. A Spectroscopic Study of Electrochemical Nitrogen and Nitrate Reduction on Rhodium Surfaces. *Angew. Chem., Int. Ed.* **2020**, *59* (26), 10479−10483.

(12) Jiang, X.; Engelhard, M.; Ataka, K.; Heberle, J. Molecular Impact of the Membrane Potential on the Regulatory Mechanism of Proton Transfer in Sensory Rhodopsin II. *J. Am. Chem. Soc.* **2010**, *132* (31), 10808−10815.
(13) Neubrech, F.; Huck, C.; Weber, K.; Pucci, A.; Giessen, H. Surface-Enhanced Infrared Spectroscopy Using Resonant Nanoantennas. *Chem. Rev.* **2017**, *117* (7), 5110−5145.
(14) Kozuch, J.; Ataka, K.; Heberle, J. Surface-enhanced infrared absorption spectroscopy. *Nat. Rev. Methods Primers* **2023**, *3* (1), 70.
(15) John-Herpin, A.; Tittl, A.; Kuhner, L.; Richter, F.; Huang, S. H.; Shvets, G.; Oh, S.-H.; Altug, H. Metasurface-Enhanced Infrared Spectroscopy: An Abundance of Materials and Functionalities. *Adv. Mater.* **2023**, *35* (34), No. 2110163.
(16) Srajer, J.; Schwaighofer, A.; Ramer, G.; Rotter, S.; Guenay, B.; Kriegner, A.; Knoll, W.; Lendl, B.; Nowak, C. Double-layered nanoparticle stacks for surface enhanced infrared absorption spectroscopy. *Nanoscale* **2014**, *6* (1), 127−131.
(17) Dong, L. L.; Yang, X.; Zhang, C.; Cerjan, B.; Zhou, L. N.; Tseng, M. L.; Zhang, Y.; Alabastri, A.; Nordlander, P.; Halas, N. J. Nanogapped Au Antennas for Ultrasensitive Surface-Enhanced Infrared Absorption Spectroscopy. *Nano Lett.* **2017**, *17* (9), 5768−5774.
(18) Adato, R.; Altug, H. In-situ Ultra-Sensitive Infrared Absorption Spectroscopy of Biomolecule Interactions In Real Time with Plasmonic Nanoantennas. *Nat. Commun.* **2013**, *4* (4), 2154.
(19) Yang, X.; Sun, Z.; Low, T.; Hu, H.; Guo, X.; García de Abajo, F. J.; Avouris, P.; Dai, Q. Nanomaterial-Based Plasmon-Enhanced Infrared Spectroscopy. *Adv. Mater.* **2018**, *30* (20), No. e1704896.
(20) Semenyshyn, R.; Hentschel, M.; Stanglmair, C.; Teutsch, T.; Tarin, C.; Pacholski, C.; Giessen, H.; Neubrech, F. In Vitro Monitoring Conformational Changes of Polypeptide Monolayers Using Infrared Plasmonic Nanoantennas. *Nano Lett.* **2019**, *19* (1), 1−7.
(21) Tittl, A.; John-Herpin, A.; Leitis, A.; Arvelo, E. R.; Altug, H. Metasurface-Based Molecular Biosensing Aided by Artificial Intelligence. *Angew. Chem., Int. Ed.* **2019**, *58* (42), 14810−14822.
(22) Li, J.; Li, J.; Yan, Z. D.; Ding, X. L.; Xia, X. H. Revealing the Hydrogen Bonding Interaction of DNA with Unnatural Bases via Plasmonic Antenna Enhanced Infrared Spectroscopy. *J. Phys. Chem. Lett.* **2021**, *12* (42), 10255−10261.
(23) Li, D.; Xu, C.; Xie, J.; Lee, C. Research Progress in Surface-Enhanced Infrared Absorption Spectroscopy: From Performance Optimization, Sensing Applications, to System Integration. *Nanomaterials* **2023**, *13* (16), 2377.
(24) Limaj, O.; Etezadi, D.; Wittenberg, N. J.; Rodrigo, D.; Yoo, D.; Oh, S.-H.; Altug, H. Infrared Plasmonic Biosensor for Real-Time and Label-Free Monitoring of Lipid Membranes. *Nano Lett.* **2016**, *16* (2), 1502−1508.
(25) Etezadi, D.; Warner, J. B.; Lashuel, H. A.; Altug, H. Real-Time in situ Secondary Structure Analysis of Protein Monolayer with Mid-Infrared Plasmonic Nanoantennas. *ACS Sens.* **2018**, *3* (6), 1109−1117.
(26) Li, J.; Wu, D.; Li, J.; Zhou, Y.; Yan, Z.; Liang, J.; Zhang, Q. Y.; Xia, X. H. Ultrasensitive Plasmon-Enhanced Infrared Spectroelectrochemistry. *Angew. Chem., Int. Ed.* **2024**, *63* (11), No. e202319246.
(27) Yao, Y.; Chen, W.; Du, Y.; Tao, Z.; Zhu, Y.; Chen, Y.-X. An Electrochemical in Situ Infrared Spectroscopic Study of Graphene/Electrolyte Interface under Attenuated Total Reflection Configuration. *J. Phys. Chem. C* **2015**, *119* (39), 22452−22459.
(28) Huck, C.; Vogt, J.; Sendner, M.; Hengstler, D.; Neubrech, F.; Pucci, A. Plasmonic Enhancement of Infrared Vibrational Signals: Nanoslits versus Nanorods. *ACS Photonics* **2015**, *2* (10), 1489−1497.
(29) Bohme, A.; Sterl, F.; Kath, E.; Ubl, M.; Manninen, V.; Giessen, H. Electrochemistry on Inverse Copper Nanoantennas: Active Plasmonic Devices with Extraordinarily Large Resonance Shift. *ACS Photonics* **2019**, *6* (8), 1863−1868.
(30) Berger, L. M.; Duportal, M.; Menezes, L. d. S.; Cortés, E.; Maier, S. A.; Tittl, A.; Krischer, K. Improved In Situ Characterization of Electrochemical Interfaces Using Metasurface-Driven Surface-Enhanced IR Absorption Spectroscopy. *Adv. Funct. Mater.* **2023**, *33* (25), No. 2300411.
(31) Duportal, M.; Berger, L. M.; Maier, S. A.; Tittl, A.; Krischer, K. Multi-band Metasurface-Driven Surface-Enhanced Infrared Absorption Spectroscopy for Improved Characterization of in-Situ Electrochemical Reactions. *ACS Photonics* **2024**, *11* (2), 714−722.
(32) Adato, R.; Yanik, A. A.; Amsden, J. J.; Kaplan, D. L.; Omenetto, F. G.; Hong, M. K.; Erramilli, S.; Altug, H. Ultra-Sensitive Vibrational Spectroscopy of Protein Monolayers with Plasmonic Nanoantenna Arrays. *Proc. Natl. Acad. Sci. U. S. A.* **2009**, *106* (46), 19227−19232.
(33) Hoffmann, J. M.; Yin, X.; Richter, J.; Hartung, A.; Maß, T. W. W.; Taubner, T. Low-Cost Infrared Resonant Structures for Surface-Enhanced Infrared Absorption Spectroscopy in the Fingerprint Region from 3 to 13 μm. *J. Phys. Chem. C* **2013**, *117* (21), 11311−11316.
(34) Chang, Y. C.; Lu, S. C.; Chung, H. C.; Wang, S. M.; Tsai, T. D.; Guo, T. F. High-Throughput Nanofabrication of Infra-Red and Chiral Metamaterials Using Nanospherical-Lens Lithography. *Sci. Rep.* **2013**, *3* (1), 3339.
(35) Neubrech, F.; Pucci, A.; Cornelius, T. W.; Karim, S.; Garcia-Etxarri, A.; Aizpurua, J. Resonant Plasmonic and Vibrational Coupling in a Tailored Nanoantenna for Infrared Detection. *Phys. Rev. Lett.* **2008**, *101* (15), No. 157403.
(36) Yi, J.; You, E.-M.; Ding, S.-Y.; Tian, Z.-Q. Unveiling the Molecule−Plasmon Interactions in Surface-Enhanced Infrared Absorption Spectroscopy. *Natl. Sci. Rev.* **2020**, *7* (7), 1228−1238.
(37) Pucci, A.; Kost, F.; Fahsold, G.; Jalochowski, M. Infrared Spectroscopy of Pb Layer Growth on Si (111). *Phys. Rev. B* **2006**, *74* (12), No. 125428.
(38) Lovrinčić, R.; Pucci, A. Infrared Optical Properties of Chromium Nanoscale Films with a Phase Transition. *Phys. Rev. B* **2009**, *80* (20), No. 205404.
(39) Rodrigo, D.; Tittl, A.; Ait-Bouziad, N.; John-Herpin, A.; Limaj, O.; Kelly, C.; Yoo, D.; Wittenberg, N. J.; Oh, S.-H.; Lashuel, H. A.; Altug, H. Resolving Molecule-Specific Information in Dynamic Lipid Membrane Processes With Multi-Resonant Infrared Metasurfaces. *Nat. Commun.* **2018**, *9* (1), 2160.
(40) Rodrigo, D.; Tittl, A.; John-Herpin, A.; Limaj, O.; Altug, H. Self-Similar Multiresonant Nanoantenna Arrays for Sensing from Near- to Mid-Infrared. *ACS Photonics* **2018**, *5* (12), 4903−4911.
(41) Rodrigo, D.; Limaj, O.; Janner, D.; Etezadi, D.; García de Abajo, F. J.; Pruneri, V.; Altug, H. Mid-Infrared Plasmonic Biosensing With Graphene. *Science* **2015**, *349* (6244), 165−168.
(42) Karst, J.; Floess, M.; Ubl, M.; Dingler, C.; Malacrida, C.; Steinle, T.; Ludwigs, S.; Hentschel, M.; Giessen, H. Electrically Switchable Metallic Polymer Nanoantennas. *Science* **2021**, *374* (6567), 612−616.
(43) Wu, C.; Guo, X.; Duan, Y.; Lyu, W.; Hu, H.; Hu, D.; Chen, K.; Sun, Z.; Gao, T.; Yang, X.; Dai, Q. Ultrasensitive Mid-Infrared Biosensing in Aqueous Solutions with Graphene Plasmons. *Adv. Mater.* **2022**, *34* (27), No. 2110525.
(44) Zheng, M. S.; Sun, S. G.; Chen, S. P. Abnormal Infrared Effects and Electrocatalytic Properties of Nanometer Scale Thin Film of PtRu Alloys for CO Adsorption and Oxidation. *J. Appl. Electrochem.* **2001**, *31* (7), 749−757.
(45) Su, Z.-F.; Sun, S.-G.; Wu, C.-X.; Cai, Z.-P. Study of Anomalous Infrared Properties of Nanomaterials Through Effective Medium Theory. *J. Chem. Phys.* **2008**, *129* (4), No. 044707.
(46) Neubrech, F.; Beck, S.; Glaser, T.; Hentschel, M.; Giessen, H.; Pucci, A. Spatial Extent of Plasmonic Enhancement of Vibrational Signals in the Infrared. *ACS Nano* **2014**, *8* (6), 6250−6258.
(47) Eilers, P. H. C. A Perfect Smoother. *Anal. Chem.* **2003**, *75* (14), 3631−3636.
(48) Vogt, J.; Huck, C.; Neubrech, F.; Toma, A.; Gerbert, D.; Pucci, A. Impact of the Plasmonic Near- and Far-Field Resonance-Energy Shift on the Enhancement of Infrared Vibrational Signals. *Phys. Chem. Chem. Phys.* **2015**, *17* (33), 21169−21175.
(49) Hu, X.; Lo, T. W.; Mancini, A.; Gubbin, C. R.; Martini, F.; Zhang, J.; Gong, Z.; Politi, A.; De Liberato, S.; Zhang, X.; et al. Near-

Field Nano-Spectroscopy of Strong Mode Coupling in Phonon-Polaritonic Crystals. *Appl. Phys. Rev.* **2022**, *9* (2), No. 021414.
(50) Yeung, C.; Tsai, J.-M.; King, B.; Pham, B.; Ho, D.; Liang, J.; Knight, M. W.; Raman, A. P. Multiplexed Supercell Metasurface Design and Optimization With Tandem Residual Networks. *Nanophotonics* **2021**, *10* (3), 1133−1143.
(51) Zheng, B.; Yang, X.; Li, J.; Shi, C. F.; Wang, Z. L.; Xia, X. H. Graphene Plasmon-Enhanced IR Biosensing for in situ Detection of Aqueous-Phase Molecules with an Attenuated Total Reflection Mode. *Anal. Chem.* **2018**, *90* (18), 10786−10794.

https://doi.org/10.1021/acsmeasuresciau.4c00048
ACS Meas. Sci. Au 2024, 4, 606−614